SUB-AMBIENT CONTROLLED TURBULENCE EFFECTS ON DISCHARGE STABILIZATION FOR LASER APPLICATIONS

Howard Allen Post

NAVAL POSTGRADUATE SCHOOL
Monterey, California

THESIS

SUB-AMBIENT CONTROLLED TURBULENCE
EFFECTS ON DISCHARGE STABILIZATION FOR
LASER APPLICATIONS

by

Howard Allen Post

September 1976

Thesis Advisor: Oscar Biblarz

SECURITY CLASSIFICATION OF THIS PAGE *(When Data Entered)*

REPORT DOCUMENTATION PAGE

READ INSTRUCTIONS BEFORE COMPLETING FORM

1. REPORT NUMBER

2. GOVT ACCESSION NO.

3. RECIPIENT'S CATALOG NUMBER

4. TITLE *(and Subtitle)*
Sub-Ambient Controlled Turbulence Effects on Discharge Stabilization for Laser Applications

5. TYPE OF REPORT & PERIOD COVERED
Master's Thesis
September 1976

6. PERFORMING ORG. REPORT NUMBER

7. AUTHOR(s)
Howard Allen Post

8. CONTRACT OR GRANT NUMBER(s)

9. PERFORMING ORGANIZATION NAME AND ADDRESS
Naval Postgraduate School
Monterey, California 93940

10. PROGRAM ELEMENT, PROJECT, TASK AREA & WORK UNIT NUMBERS

11. CONTROLLING OFFICE NAME AND ADDRESS
Naval Postgraduate School
Monterey, California 93940

12. REPORT DATE
September, 1976

13. NUMBER OF PAGES
64

14. MONITORING AGENCY NAME & ADDRESS(if different from Controlling Office)
Naval Postgraduate School
Monterey, California 93940

15. SECURITY CLASS. *(of this report)*
Unclassified

15a. DECLASSIFICATION/DOWNGRADING SCHEDULE

16. DISTRIBUTION STATEMENT *(of this Report)*
Approved for public release; distribution unlimited.

17. DISTRIBUTION STATEMENT *(of the abstract entered in Block 20, if different from Report)*

18. SUPPLEMENTARY NOTES

19. KEY WORDS *(Continue on reverse side if necessary and identify by block number)*
turbulent flow
electric discharge laser
sub-ambient pressure

20. ABSTRACT *(Continue on reverse side if necessary and identify by block number)*

This work deals with the effect of reduced pressure in a controlled turbulent flow on electric discharge stabilization. A converging-diverging nozzle was designed and fabricated to provide a device for investigating this phenomenon. Turbulence was generated by perforated plates designed with a geometry that had proven to be successful in previous controlled turbulent

DD FORM 1 JAN 73 1473 EDITION OF 1 NOV 65 IS OBSOLETE
(Page 1) S/N 0102-014-6601 |

SECURITY CLASSIFICATION OF THIS PAGE *(When Data Entered)*

20. Abstract (Cont'd)

work. Turbulence and discharge data are presented along with photographs of the discharge for no flow, laminar flow and turbulent flow.

Sub-Ambient Controlled Turbulence Effects on Discharge Stabilization for Laser Applications

by

Howard Allen Post
Lieutenant, United States Navy
B.S., Northrop Institute of Technology, 1967

Submitted in partial fulfillment of the
requirements for the degree of

MASTER OF SCIENCE IN AERONAUTICAL ENGINEERING

from the
NAVAL POSTGRADUATE SCHOOL
September 1976

ABSTRACT

This work deals with the effect of reduced pressure in a controlled turbulent flow on electric discharge stabilization. A converging-diverging nozzle was designed and fabricated to provide a device for investigating this phenomenon. Turbulence was generated by perforated plates designed with a geometry that had proven to be successful in previous controlled turbulent work. Turbulence and discharge data are presented along with photographs of the discharge for no flow, laminar flow and turbulent flow.

TABLE OF CONTENTS

LIST OF ILLUSTRATIONS

Figure

ACKNOWLEDGEMENTS

The author gratefully acknowledges Associate Professor Oscar Biblarz for the encouragement and guidance he furnished during the course of this investigation. Further acknowledgements are extended to the technical staff of the Department of Aeronautics under R. Besel and T. Dunton, particularly to R. Ramaker for his assistance in the fabrication of equipment used in this study and to C. Gordon and J. Hammer for their assistance in calibration of diagnostic equipment. Finally, acknowledgements to my wife and children for their patience, understanding and encouragement.

I. INTRODUCTION

Several classes of electric discharge gas laser devices are currently under investigation. (Ref. 1) A stagnant or no flow device accomplishes heat removal and discharge stabilization by diffusion to cavity walls. Maximum practical power capability for this class of lasers is approximately 500 watts (W) with a 10 meter (m) glass tube. Another one incorporates gas flow for convective cooling and discharge stabilization by diffusion to cavity walls. These devices have a practical power capability of 5kW with a 7 m glass tube. A similar class, using convective cooling, increases discharge stabilization by various pre-ionization techniques with power capabilities greater than 10kW.

Recent work with turbulent flow for discharge stabilization adds a fourth class of laser devices which have promising power capability. Biblarz and Nelson (Ref. 2) report significant discharge power increases with ambient pressure turbulent flow. Low pressure (80-200 Torr) turbulent flow studied by Wiegand and Nighan (Ref. 3) found increased discharge stabilization as a consequence of the turbulence. Another low pressure study by Wasserstrom, Crispin, Rom and Shwartz (Ref. 4) used a transverse secondary

flow to create vortical flow. They also found that vortex flow had a significant effect on discharge stabilization.

The power capability of an electric discharge convective laser is scalable with mass flow rate (Ref. 5). The mass flow rate can be increased by increasing density, discharge area and velocity. Elevated pressure causes difficulty with discharge stabilization but more power can be coupled into the lasing mixture. No-flow breakdown data at different discharge pressures for 4 cm and 8 cm electrode gaps are presented by Loeb in Reference 6. Using these data, breakdown power for increasing pressure is shown in Figure 1. A single maximum is reached for a given gap length, indicating an optimum discharge pressure. The purpose of this project is to investigate the effect of sub-ambient controlled turbulence flow on discharge performance in the range above 450 Torr.

Section II deals with selecting an economically fabricated device to explore the desired region and discusses the general philosophy supporting its design. A complete description of the entire apparatus is presented in Section III. The experiment was divided into two primary areas, turbulence tests and discharge tests, which are discussed in Section IV. The results of the experiment and conclusions,

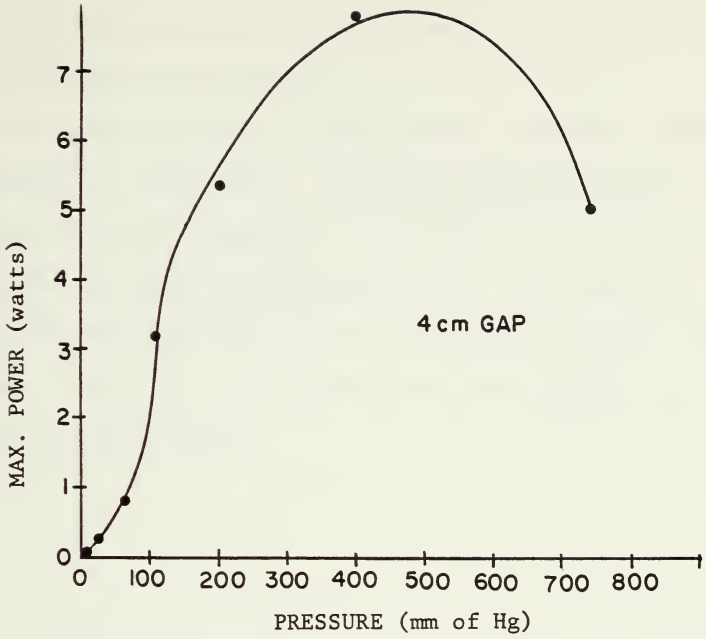

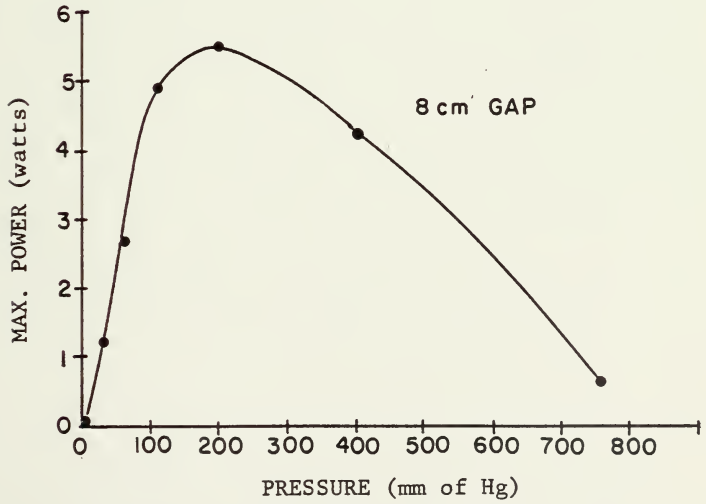

Figure 1. Breakdown Power Versus Pressure (Loeb Data, Ref. 6)

with some recommendations for improvement, are found in Sections V and VI respectively.

An interesting model of space charge convection effects is presented in Reference 7. Numerous experiments were conducted during this project to provide data to help establish and support the proposed model. Air was used for the discharge medium in all tests performed during this project. A CO_2, N_2 and He mixture would be expected to produce superior results.

II. REDUCED PRESSURE SYSTEM DESIGN CRITERIA

The design for reducing pressure in the electric discharge test section resulted from a preliminary study of two gasdynamic methods. First, the possibility of using a converging nozzle, such that the inlet was open to atmospheric air and the exit coupled to an evacuated reservoir, was considered. A pressure ratio of sixty per cent of atmospheric air could be obtained in the test section. However, the flow rate required to produce this pressure reduction combined with the need for at least a two minute run time dictated the use of a reservoir and vacuum pump much larger than was locally available. This approach, therefore, was subsequently abandoned.

An alternative method which consists of using the flow characteristics of a converging-diverging nozzle was adopted. The system is driven by compressed air at the inlet, with the diffuser exit open to atmospheric air. A short, constant area section at the throat of the nozzle houses the electrodes for the electric discharge test section. The turbulence generating plates used in the experiment present approximately fifty per cent area blockage to the flow. To avoid choking the flow at the plate prior to reaching

desired test section conditions, a plate chamber was located upstream of the test section in the converging portion of the nozzle.

The specific design of the nozzle was based on three required features. First, a pressure ratio of sixty per cent of atmospheric air and Mach 0.95 were the desired maximum operating conditions in the test section. Test section conditions would be reached when flow through the plate chamber, which housed a plate with fifty per cent area blockage, reaches Mach 0.3. The section linking the plate chamber with the test section had to be as short as possible, thereby keeping the turbulence generating plate within reasonable range of the test section. With this configuration discharge density would be a function of velocity but it was concluded that the effect of these two parameters on discharge stability could be separated. Details of the various sections are presented in Section III.

It is known that vortex stretching occurs in accelerated flow of a wind-tunnel contraction, thus attenuating the low frequency, high energy turbulent spectrum of the flow. (Ref. 8) The location of the turbulence generating plate inherently placed the produced turbulent flow in this adverse environment. Low frequency, high energy turbulence is known to have a stabilizing effect on the discharge. (Ref. 2)

It was felt that the plate hole dimensions could be altered to compensate for the attenuation and that the plate was located close enough to the test section to insure adequate turbulent flow through the discharge. This was later found to be incorrect. Turbulence decay was measured and is discussed in Section V.

Since breakdown conditions are slightly variable with changes in water vapor partial pressure (Ref. 9), a study was conducted to determine a method for drying the air supply. Chemical dryers provide the most effective means for drying moist air but commercial products capable of accommodating the expected flow rates are large, expensive units thus precluding their use. To provide consistency of measured data, the effect of relative humidity had to be taken into account. It was decided that breakdown voltage data would be corrected to a standard humidity of 0.6085 inches of mercury vapor pressure by applying a correction factor determined from curves presented in Reference 9. The procedure used for determining the partial pressure of water vapor in the discharge region, and the correction factor curve, are presented in Appendix A. Recent work related to water vapor effects on breakdown voltage can be found in Reference 10.

III. EXPERIMENTAL APPARATUS

The experimental apparatus is composed of three major subsystems. These subsystems include an air flow system, a variable high-voltage D.C. discharge circuit, and a turbulence measurement system. Figure 2 is a photograph of the laboratory and most of the equipment used in the experiment.

A. THE FLOW SYSTEM

The flow system consists of an air compressor, water-cooler heat exchanger, flow rate control valves, a plenum section and a converging-diverging nozzle. Figure 3 is a schematic of the entire flow system. Air supply is provided by a Carrier three-stage centrifugal compressor with a 4000 ft^3/min. capability at a maximum pressure of two atmospheres. The flow is directed through a water-cooler heat exchanger that maintains a stabilized flow temperature at approximately 90^oF.

Three gate valves are used to control the flow rate through the test section. Two of these valves are located downstream of the heat exchanger and are the primary control valves for the flow. It was determined that the flow choked in the heat exchange when the primary valves were set for

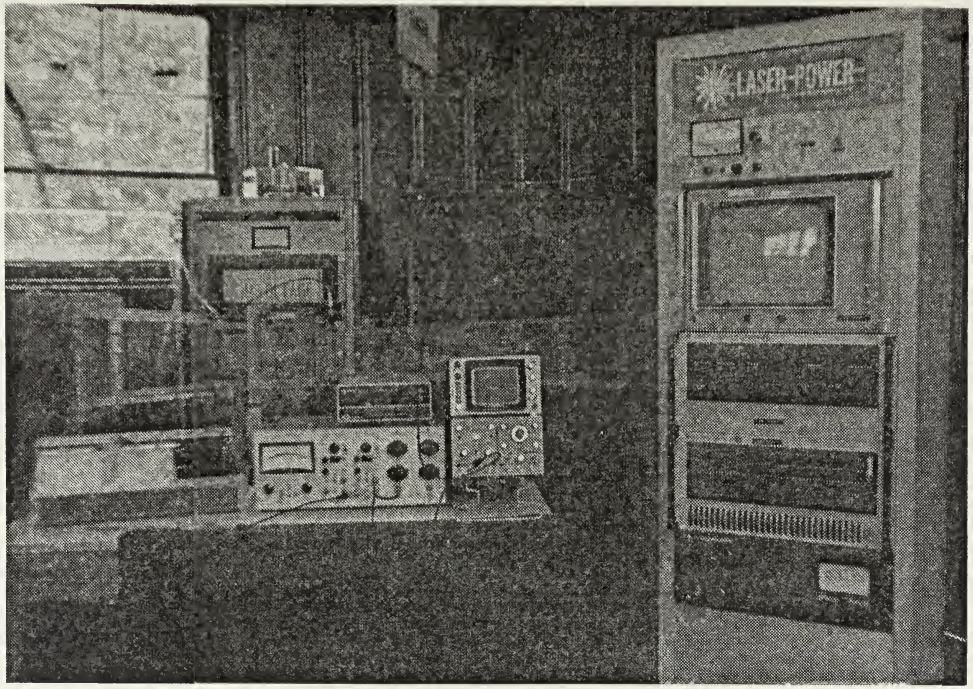

Figure 2. Laboratory Equipment

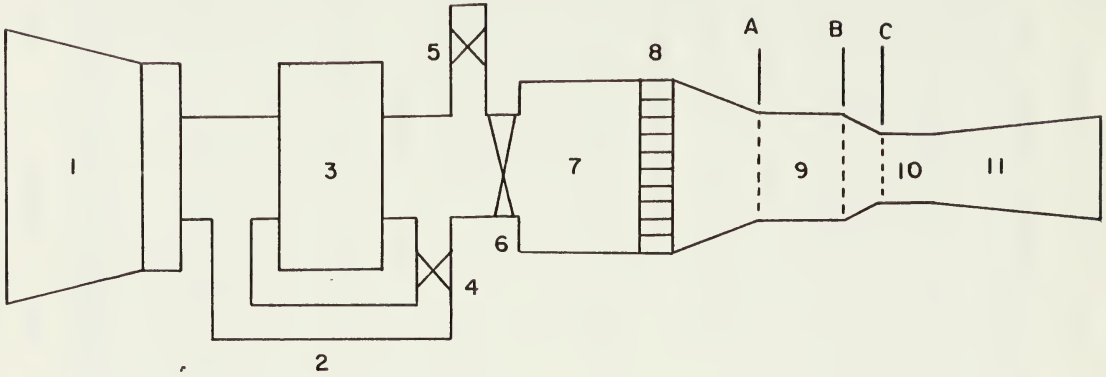

1. Compressor
2. Heat Exchange By-Pass
3. Heat Exchanger
4. Gate Valve
5. Gate Valve
6. Gate Valve
7. Plenum
8. Honeycomb
9. Plate Chamber
10. Test Section
11. Diffuser

NOTE: A, B, and C are locations discussed in the text.

Figure 3. Flow System Schematic

maximum flow and this, therefore, necessitated the installation of a heat exchanger by-pass controlled by the third gate valve. The by-pass eliminates the problem and full flow is available.

A plexiglass plenum chamber used in Reference 11 was incorporated into this apparatus but it catastrophically failed during early operation and was subsequently replaced with a 3/4 in. thick, plywood structure. The plywood plenum joints were glued and reinforced. Internal and external surfaces were sealed to prevent moisture absorption. Aluminum honeycomb inserts dampen upstream turbulence and straighten the flow in the plenum.

The converging-diverging nozzle is a plexiglass assembly of five individual sections. The assembled nozzle is shown in Figure 4. A converging section connects the original plexiglass plenum chamber to the plate chamber. The inside dimensions for the inlet, i.e., 9 in. x 9 in. were selected to integrate the new nozzle with the structure already present. The inside dimensions of the exit match that of the plate chamber.

A plate chamber houses and supports the turbulence generating plates. The chamber's cross sectional area of 20 $in.^2$ was selected so that at maximum operating conditions, i.e., Mach 0.3 flow in the plate section, the corresponding

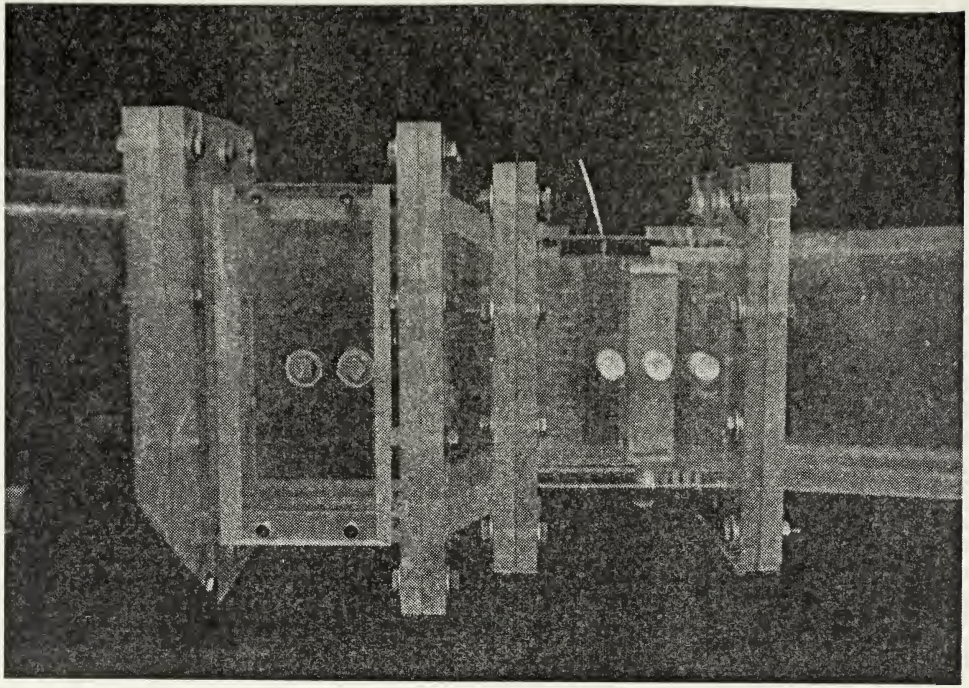

Figure 4. Nozzle Assembly

test section area (based on isentropic relations, Ref. 12) would be of sufficient size to house the electrodes. Removal of a pressure tight hatch allows easy access to the plate which, therefore, can be readily changed. The plate chamber is schematically illustrated in Figure 5.

A short converging section links the plate chamber with the test section. Its length was determined by fabrication factors and the desire to have the plate as close as possible to the test section. The test section provides support for the electrodes and includes a number of features. The cathode can be moved to provide various electrode spacings, with a minimum spacing of 2.9 cm. Numerous threaded ports in the walls of the test section provide access for diagnostic probes which are secured in position by pressure tight fittings. The test section schematic is presented in Figure 6. A photograph of the fabricated section is shown in Figure 7.

The diffuser section has an overall length of 41.18 inches and a wall divergence angle of 2.5 degrees. Tufts were placed along the diffuser wall to check visually for flow separation.

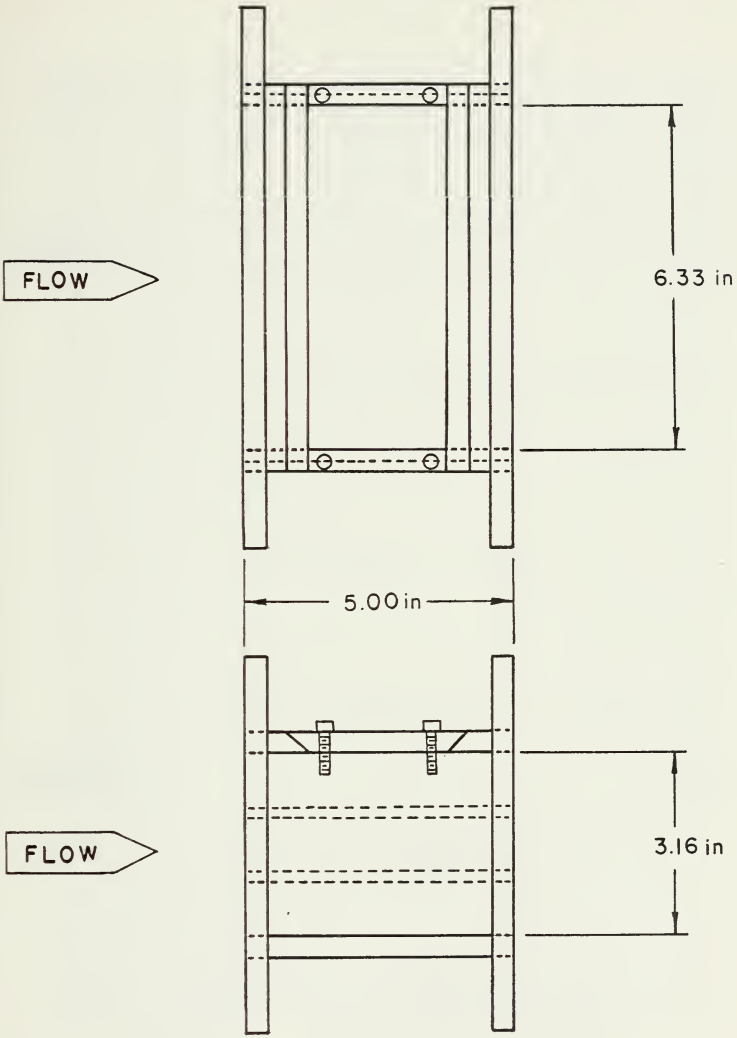

MATERIAL: 0.75 INCH PLEXIGLASS

Figure 5. Plate Chamber Schematic

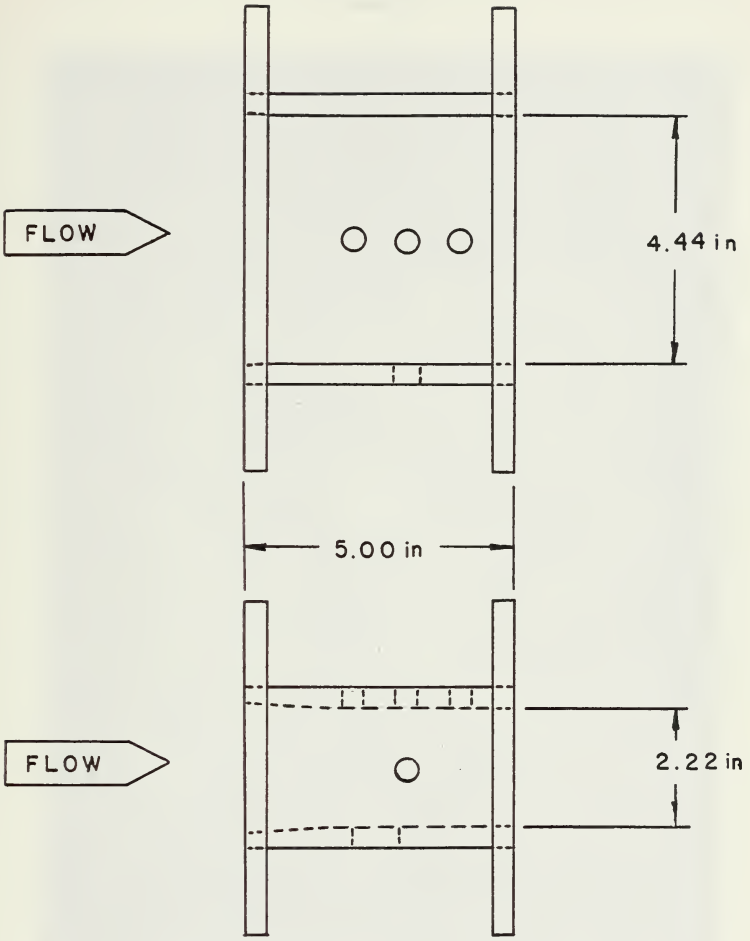

MATERIAL: 0.75 INCH PLEXIGLASS

Figure 6. Test Section Schematic

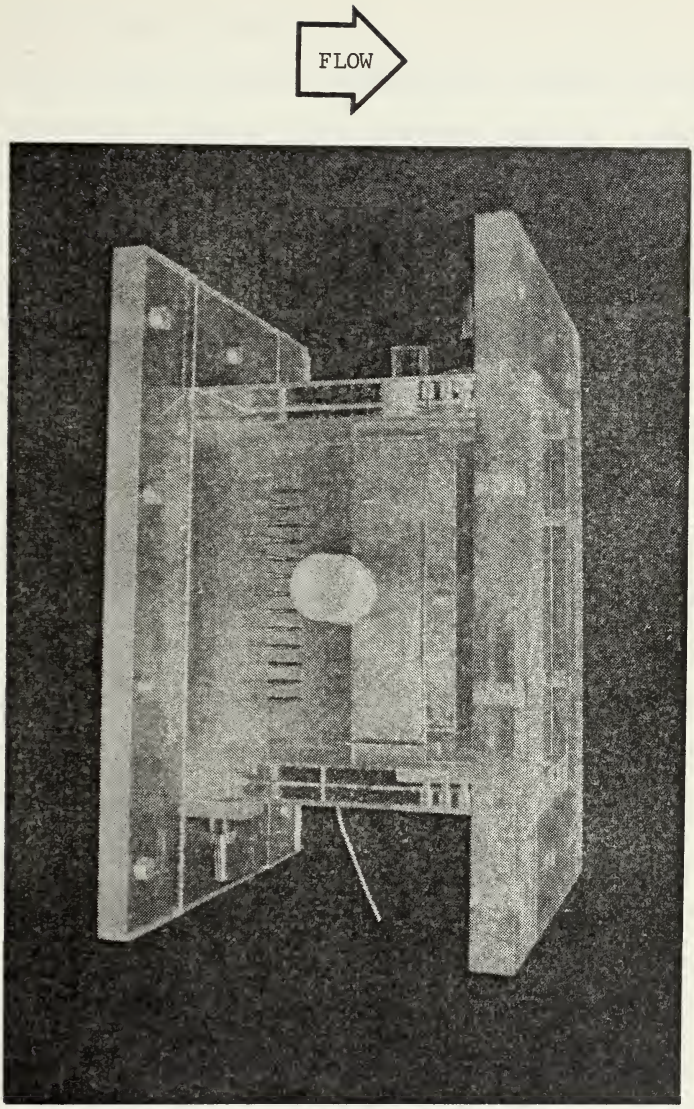

Figure 7. Test Section

B. THE DISCHARGE CIRCUIT

Three primary elements comprised the variable voltage, D.C. discharge circuit. These elements include a variable high-voltage, D.C. source, the discharge electrodes and current/voltage meters. Figure 8 is a schematic of the circuit.

Two high-voltage power supplies were available and were independently used in the experiment. A Sorenson high-voltage, D.C. power supply with a maximum output of 30 kilovolts (kV) and 20 milliamperes (mA) powered the electric discharge in most of the tests. An old Sorenson Beta high-voltage, D.C. power supply with a rated maximum output of 60kV and 50mA was also used but found capable of producing only 34kV and 18mA. The power supplies were interchanged to cross check measurements of experimental discharge power data. Excellent agreement was observed.

The discharge electrodes consist of a pin anode arrangement similar to Aunchman's (Ref. 11) and a wire grid cathode. The anode pins were made from 0.0625 inch steel wire and mounted on an airfoil machined from 0.5 to 0.125 inch brass strip. Figure 9 shows the details of the pin electrode. The wire grid cathode arrangement resulted from a series of preliminary tests utilizing Aunchman's equipment. The airfoil cathode used by Aunchman was replaced by an aluminum

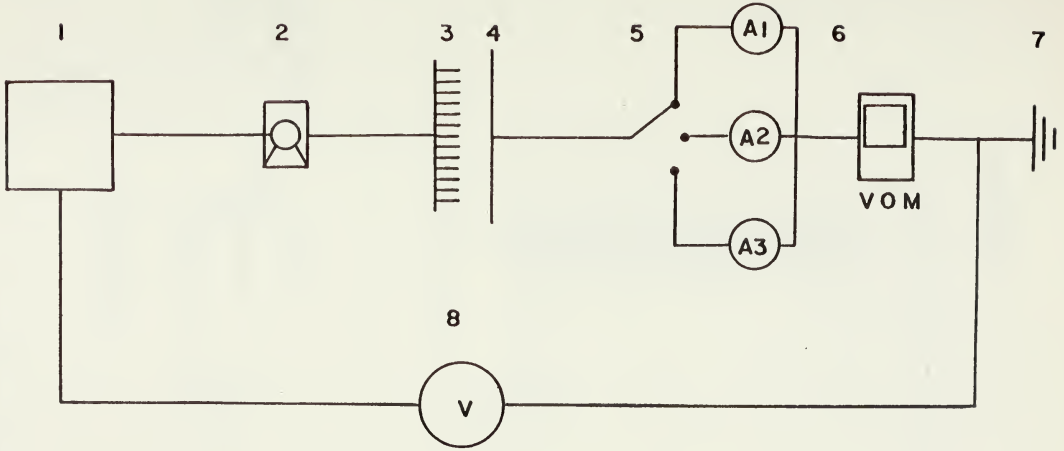

1. Power Supply
2. Oil Submerged Brass Sphere
3. Pin Anode
4. Wire Grid Cathode
5. "Make-Before-Break" Switch
6. Ammeters
7. Laboratory Ground
8. Voltmeter

Figure 8. High Voltage Discharge Circuit

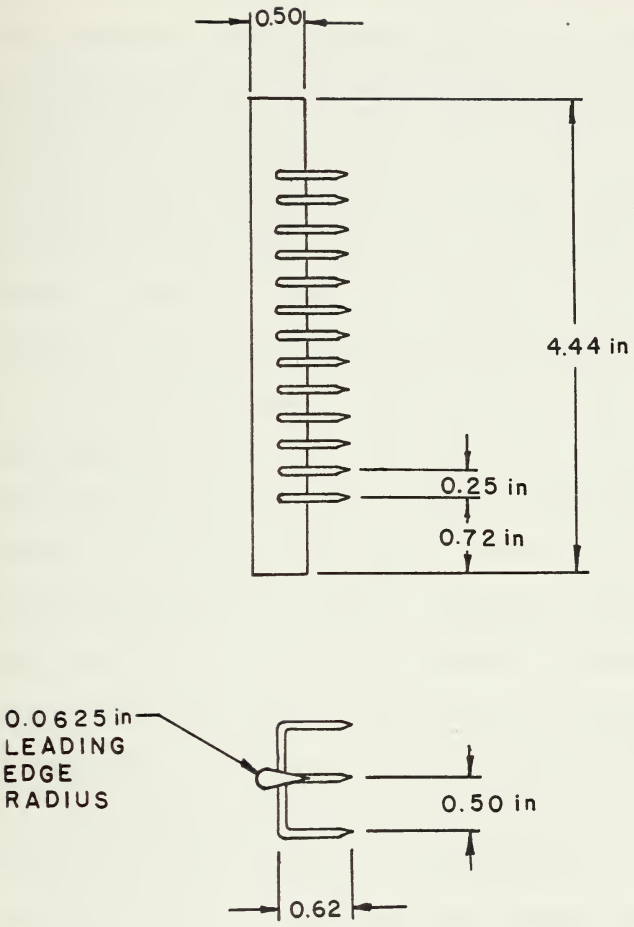

Figure 9. Pin Anode Schematic

honeycomb cathode to establish a more uniform field, and did perform slightly better than the airfoil arrangement. The honeycomb cathode was not rigid enough to withstand the flow forces and hence was replaced by a wire grid cathode which performed just as well. It was learned later that wire grid cathodes are the preferred cathode geometries of axial flow systems. (Ref. 13) A photograph of the electrodes is shown in Figure 10. Mounted on the pin anode is plate III used in the tests and described later.

Current measurements were taken with three Triplett milliammeters with ranges from 0.0 to 1.0, 10.0 and 50.0 milliamperes wired in series through a "make before break" switch. A Simpson 260 V-O-M was also used for a cross check measurement of current. Originally, discharge voltage was measured with a Sensitive Research electrostatic voltmeter but a short circuit was detected in the meter and precluded its use. The power supply control panel voltmeter readings are within one per cent of the Sensitive Research meter and it was therefore used to measure the discharge voltage. This error was taken into account when an error bar for measured breakdown voltage was determined. High-voltage leads were used throughout the circuit. Power supply connections were made through a highly polished, oil submerged, brass sphere.

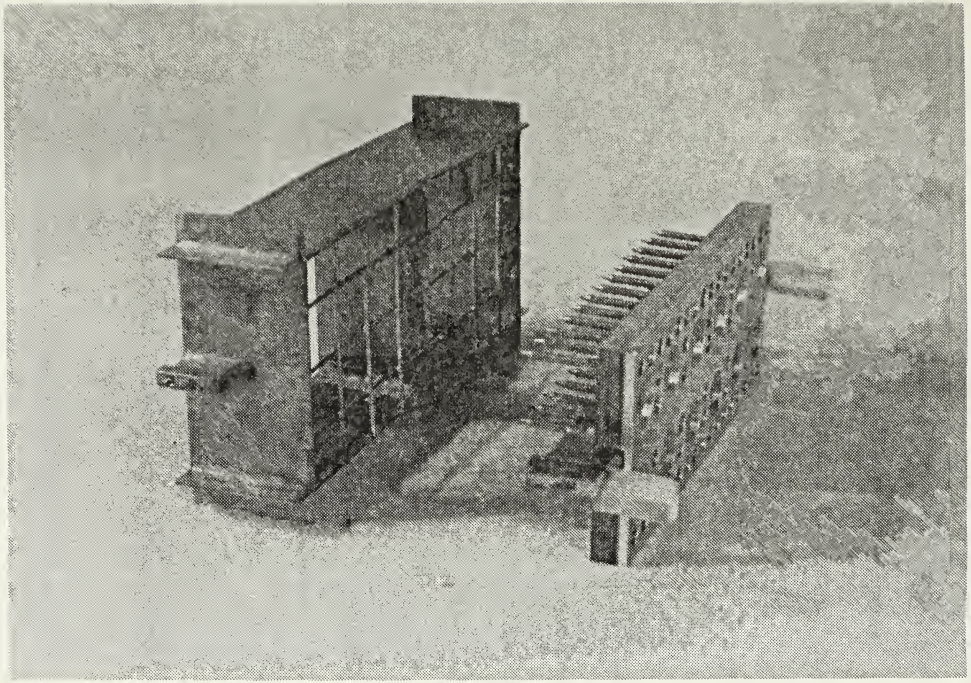

Figure 10. Electrodes

C. TURBULENCE EQUIPMENT

Turbulence diagnostic equipment includes a Thermo Systems Inc. hot wire anemometer, a Hewlett-Packard oscilloscope, a General Radio Company, Type 1921, real time analyzer and a Hewlett-Packard 7035B X-Y recorder. Hot wire probe filaments are 0.00015 inch diameter tungsten wires spot welded to the probe supporting pins. Hot wire anemometer components include a model 1051-2 monitor and power supply and a model 1054A-20 anemometer module.

The oscilloscope was used for setting and adjusting the stability and frequency response of the anemometer. Difficulty was encountered in matching probe/anemometer impedance following the procedure outlined in the operators manual. To alleviate the problem, various lengths of coaxial cables were kept on hand for coarse impedance matching, followed by fine adjustments of the anemometer. In general, the hot-wire system proved difficult to use. Considerable skill and time were required to spot weld the tungsten wires in place. The wired probes were fragile and required frequent replacement.

The real time analyzer is composed of a model 1925, 30 channel multifilter and a model 1926 multichannel RMS detector. Based on experience gained in Reference 2,

four-second integration times were used during all measurements. The X-Y recorder enables rapid and accurate data collection from the memory output of the analyzer. All equipment is grounded through a separate grounding system in the laboratory.

D. OTHER DIAGNOSTIC EQUIPMENT

A number of diagnostic instruments used in the experiment were fabricated locally. Iron-constantan and copper-constantan thermocouples were used for total temperature measurements. A pitot-static probe, using either water or mercury manometers, provided pressure data. The thermocouples and pitot-static probe were carefully calibrated at a local facility. Pressure and temperature measurements of a free jet from Mach 0 to Mach 1.0 were compared with highly accurate reference probes. The calibration procedure resulted in detection of a faulty probe, which was discarded, and permitted a high level of confidence in experimental measurements. Other diagnostic equipment was also calibrated according to operating manuals. Calibration results were used to estimate an error bar for the various measured test parameters. Error analysis is presented in Appendix B.

IV. EXPERIMENTS CONDUCTED

The experiments performed were divided into two main areas. First, turbulence spectrum sampling was required to investigate the amount of turbulence decay encountered with accelerated flow in this apparatus and to make necessary modifications. Large eddies must be present in the discharge region to have a stabilizing effect in breakdown as evidenced by Reference 1 and Reference 4. Second, maximum discharge performance was to be investigated with turbulent and non-turbulent flow. The diffuser was removed to obtain reference data at near atmospheric conditions. With the diffuser on, density reduction effects could then be studied.

A. TURBULENCE TESTS

In Reference 11, spectrum distributions were obtained for various plates. Plate 9 had produced the most intense, homogeneous turbulence distribution. However, discharge performance tests at a velocity of 200 ft/sec. (61 m/sec.) showed Plate 1-6 outperformed Plate 9. Preliminary tests using these plates and Aunchman's test section, showed that Plate 9 was superior at higher velocities. Plate 9

geometry was adopted for use in the current apparatus. The various plate modifications used are identified as Plates I, II and III. Figure 11 describes these plates in detail.

A spectrum distribution of the turbulence generated by the pin anode was recorded at a test section velocity of 200 ft/sec. (61 m/sec.). Plate I was used to investigate spectral decay associated with flow acceleration. This was accomplished by placing Plate I at the upstream end of the plate chamber. (Position A, Fig. 3). Turbulence spectrum was measured in the chamber 3.5 inches (8.89 cm) downstream of the plate. Plate I was then relocated at the downstream end of the chamber (Position B, Fig. 3) and turbulence in the test section 3.5 inches (8.89 cm) downstream of the plate was recorded. Comparing the spectra obtained by this procedure, acceleration effects on turbulence were determined. Spectrum decay was much greater than initially anticipated. Plate II was manufactured and tested in the same manner. With Plate II installed at location B, spectra in the test section were measured with and without the diffuser.

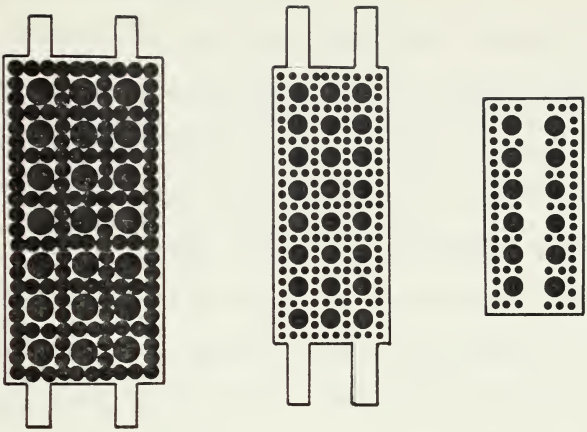

Plate I Plate II Plate III

	I	II	III
MATERIAL:	COPPER	PHENOLIC	ALUMINUM LAMINATED ON PHENOLIC
LENGTH (IN.)	6.0	5.2	3.6
WIDTH (IN.)	2.6	2.2	1.5
THICKNESS (IN.)	0.125	0.18	0.25
DIAMETER (IN.)			
LARGE HOLES:	0.50	0.375	0.375
SMALL HOLES:	0.187	0.125	0.125

Figure 11. Turbulence Generating Plates

B. DISCHARGE PERFORMANCE TESTS

This part of the experiment involved discharge power performance under the influence of the various plate and nozzle arrangements used in the turbulence tests. Three internal configurations were studied with the diffuser removed. First, maximum discharge performance with increasing velocity was measured for a no-plate, "laminar" condition. Again, maximum discharge performance with increasing velocity was recorded with Plate II installed in the plate chamber. Since power supply limitations were reached prior to obtaining optimum desired test section conditions, it was decided to manufacture Plate III and mount it on the immediate upstream edge of the pin anode. This configuration is shown in Figure 10 and the plate position is identified with position C in Figure 3. It was anticipated that the flow would choke at the plate prior to optimum discharge conditions, but it was felt that power supply limitations would be reached prior to choking. Attempts were made to obtain a turbulence spectrum of Plate III in the discharge region, but hot wire tungsten filaments could not survive this intense turbulent flow even at low velocities. All the above tests were repeated with the diffuser on.

A number of other tests involving variable voltage rates and various gap lengths were performed to provide a data basis for a model presented in Reference 7.

V. DISCUSSION OF RESULTS

Spectral data indicate that a severe low frequency turbulence decay occurs for plates positioned at location B (Fig. 3) in the accelerated flow. These data are presented in Figure 12. Comparing the unaccelerated spectrum with the accelerated spectrum of Plate I illustrates the decay encountered. Spectra shifted slightly to the right with increasing velocity as was observed in Reference 11. Plate III turbulence spectrum could not be measured, for reasons previously stated, but some partial data did show turbulence intensities above 40dB. No changes in the spectrum were observed with diffuser on and diffuser off nozzle configurations at a test section velocity of 200 ft/sec. (61 m/sec.).

Total mass flow rate through the nozzle was computed from plate chamber diagnostics. Mass flow through the discharge region was less than total mass flow because of plate and pin anode blockage. The plate does not extend from wall to wall. The width of the plate is less than the total width of the test section and thus provides a "boundary layer" slot. The slot allows higher mass flow along the walls to remove discharge waste heat and to

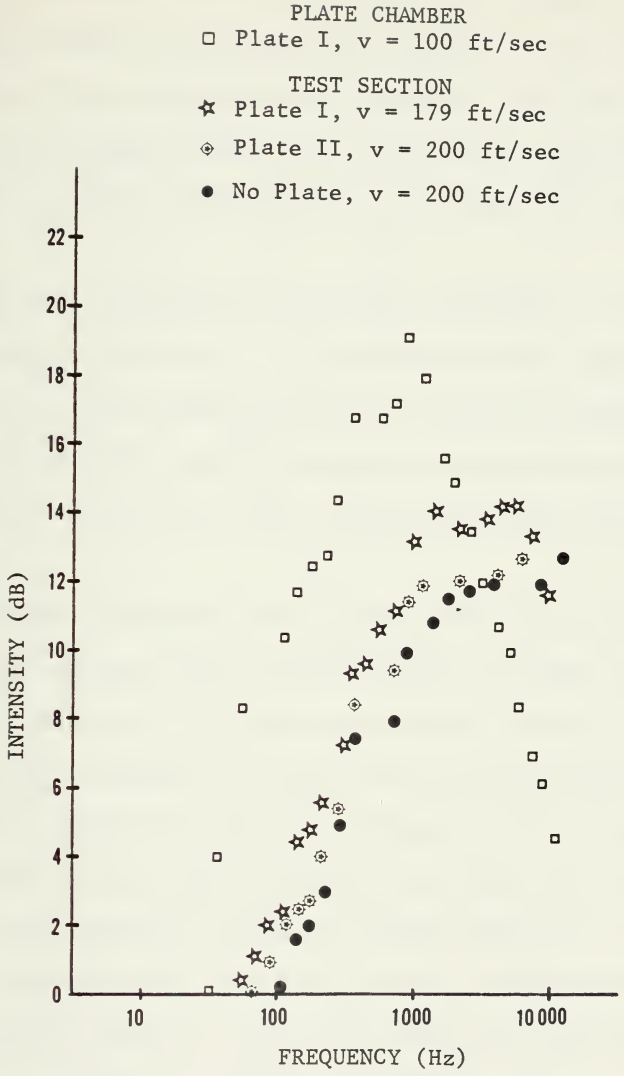

Figure 12. Turbulence Spectra

remove any water condensation. Mass flow outside the discharge volume was determined from diagnostics in that region of the test section and subtracted from the total mass flow giving the mass flow rate through the discharge volume. Figure 13 was constructed from mass flow rate data.

An error analysis for discharge performance curves is presented in Appendix B. The magnitude of the computed error bar was extremely sensitive to pressure readings. At high pressures, mercury manometers were used producing a larger error bar than the readings from the water manometers.

Maximum discharge power per mass flow rate or energy per mass obtained for no plate "laminar" flow and turbulent flow using Plate III located at position C (Fig. 3) are presented in Figure 14. These curves show an initial decrease in energy per mass to a minimum and then rapidly increase. At low mass flow rates the total power remained relatively constant causing the initial decrease. As mass flow rate increased, convective cooling, turbulence and sub-ambient density increased the stability of the discharge resulting in greater total discharge power. The model presented in Reference 7 suggests how velocity,

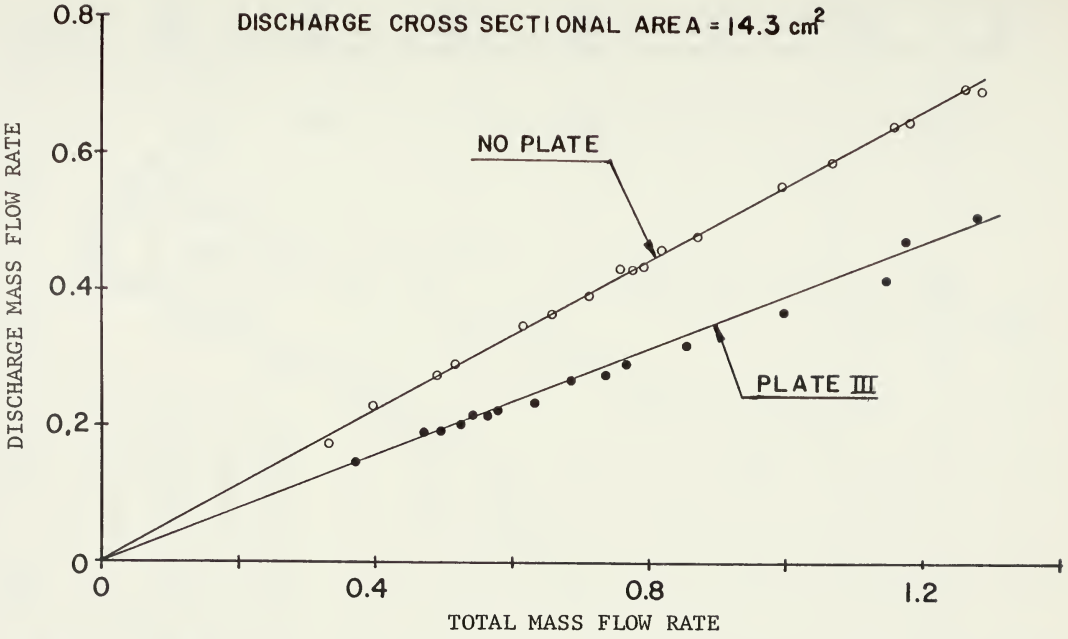

Figure 13. Mass Flow Rate Through the Discharge Versus Total Mass Flow Rate

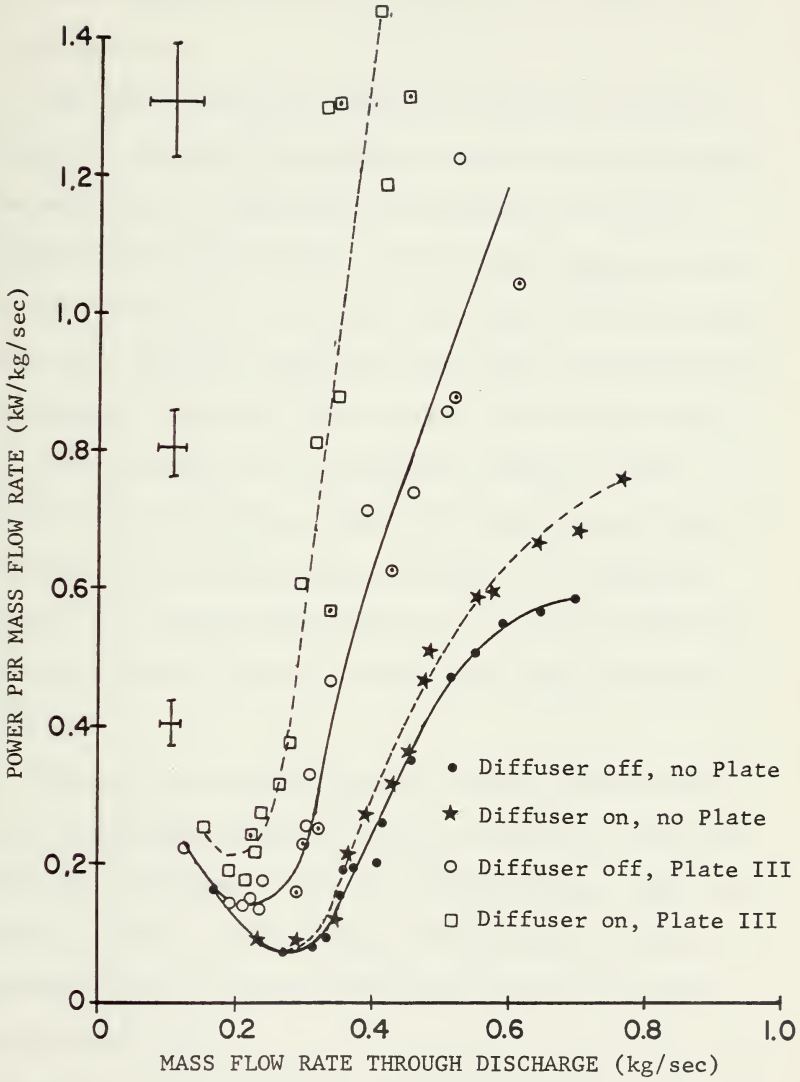

Figure 14. Power Per Mass Flow Rate Versus Mass Flow Rate Through the Discharge

turbulence and density influence discharge stability. The data presented here help support the validity of the proposed model.

Sub-ambient density effects on discharge stability caused an increase in energy per mass as was anticipated. The advantage of turbulent, sub-ambient flow can be realized from these curves. At the power supply current limited points, i.e., the last data point for each curve, more than twice the energy per unit mass was obtained for sub-ambient turbulent flow at about half the mass flow rate when compared with atmospheric "laminar" flow. Another way of looking at this is to superimpose lines of constant power on the curves of Figure 14 as shown in Figure 15. A given power level can be reached with sub-ambient turbulent flow at a much lower "cost" in mass flow rate.

Figure 14 also shows that the laminar curves appear to be approaching an upper bound on energy per unit mass while the turbulent curves are rapidly rising. Data from plates I and II were identical to the laminar curves, demonstrating the severe turbulence attenuation of the accelerated flow.

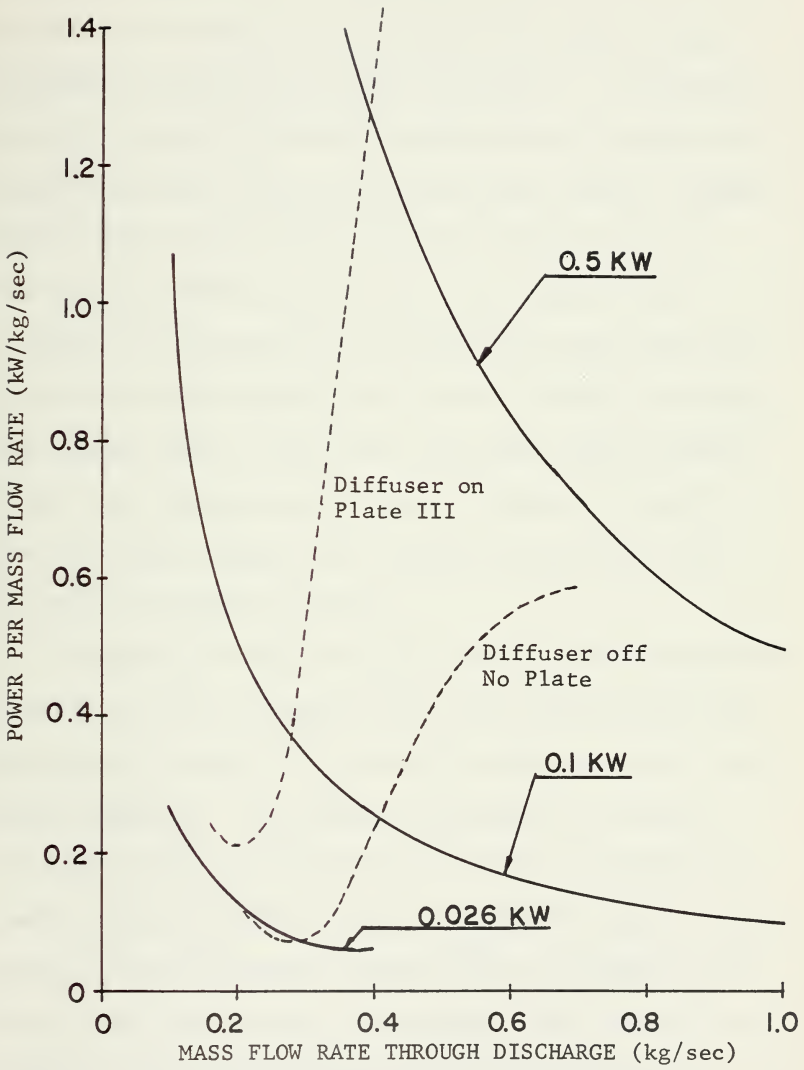

Figure 15. Constant Power Curves

An average discharge velocity was computed from discharge mass flow rates. Convective cooling and turbulent effects on discharge stability with increasing average discharge velocity can be seen in Figure 16. Increasing velocity provided convective cooling which increased discharge stability and hence greater power density. Higher power densities were obtained with turbulent flow at velocities greater than 60 m/sec. The slope of the "laminar" curve appears to be decreasing above 160 m/sec. Peak power would probably be reached at choked conditions. The extreme ends of the curves are power supply current limits, not energy density limits. Figures 17 and 18 give breakdown voltage and breakdown current data for increasing discharge velocity.

Photographs of the discharge near breakdown conditions taken for no-flow, "laminar" flow and turbulent flow are presented in Figure 19. The no-flow photograph was a ten-second exposure. The general appearance of the glow discharge shows a low intensity discharge extending between each pin and the cathode. The bright region at the bottom of the photograph resulted from a breakdown spark during the time exposure. In contrast, the "laminar" and turbulent flow photographs were one-second exposures. In

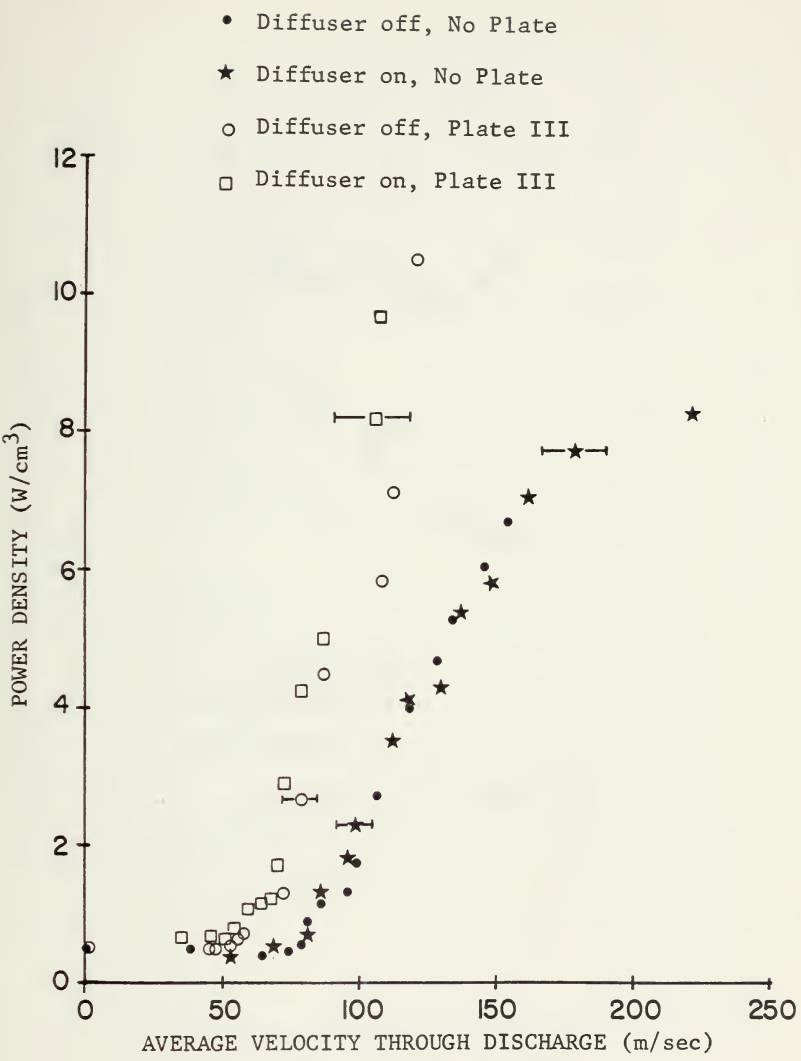

Figure 16. Power Density Versus Average Velocity Through the Discharge

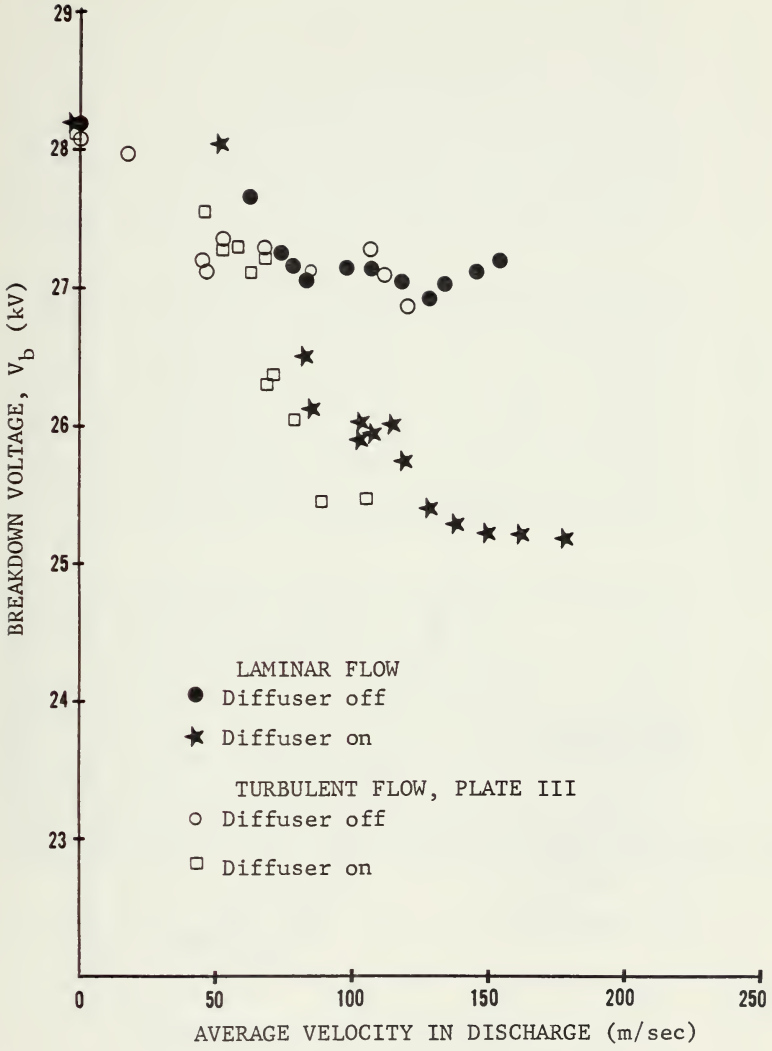

Figure 17. Breakdown Voltage Versus Average Velocity Through the Discharge

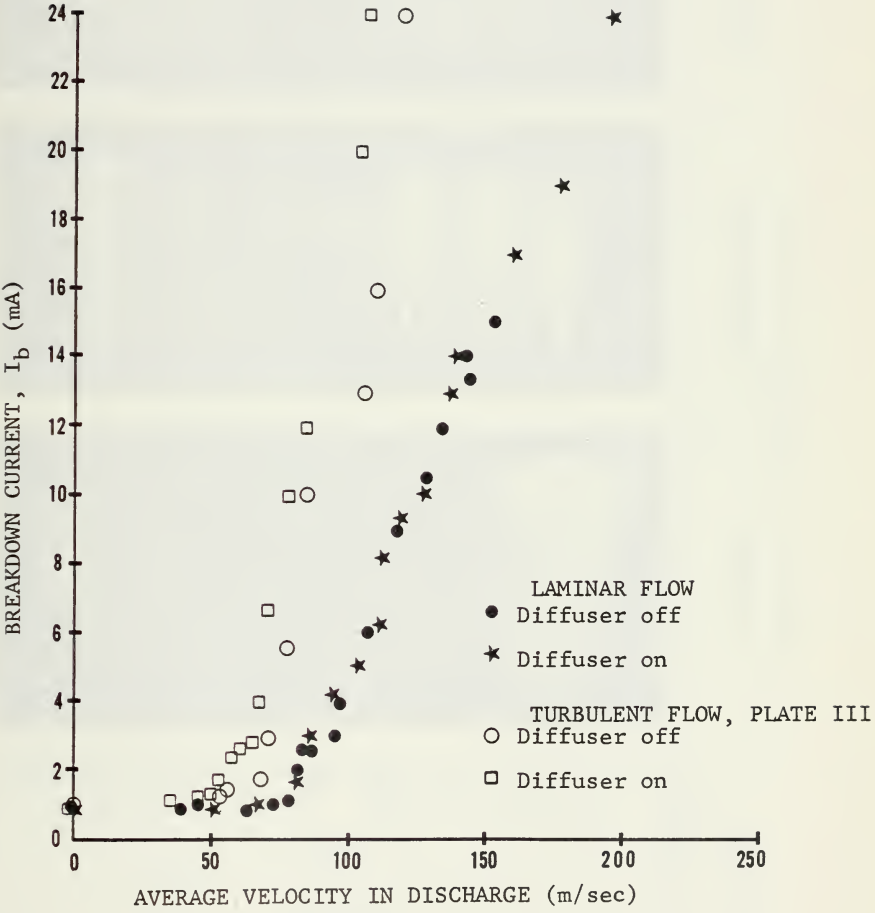

Figure 18. Breakdown Current Versus Average Velocity Through the Discharge

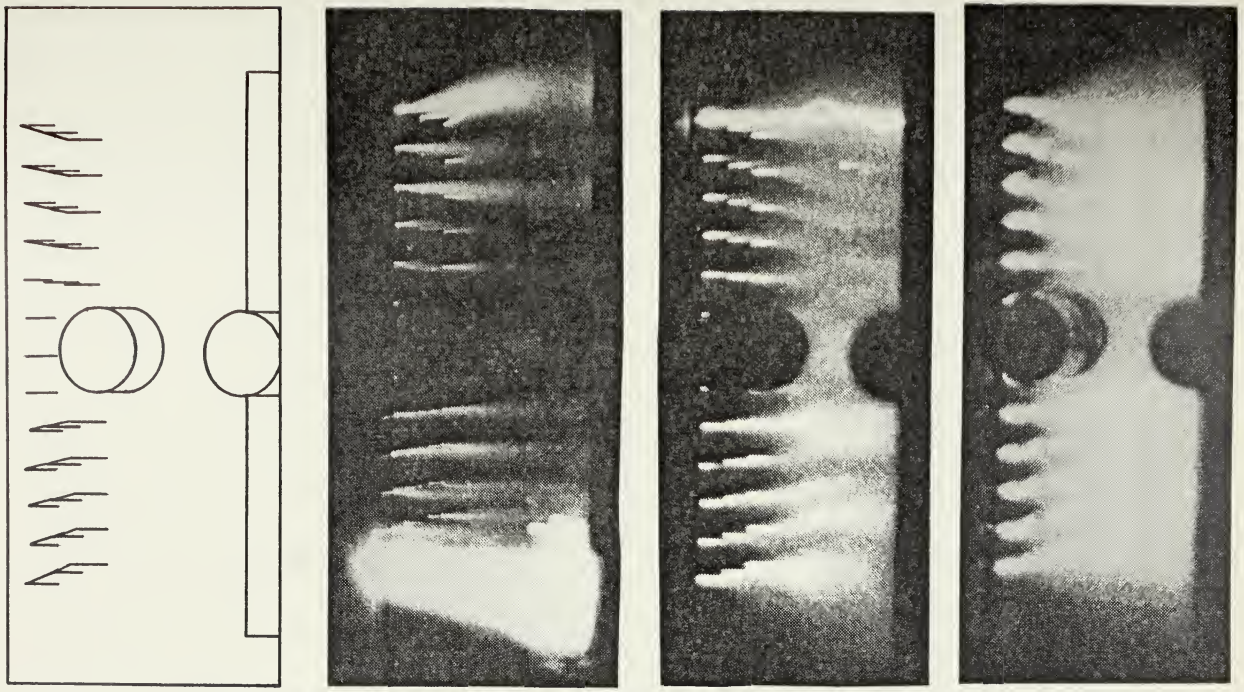

Figure 19. Discharge Appearance

the "laminar" flow photograph, the individual pin discharges were more diffused. An intense, short, narrow glow extending from the pin anode tips had developed. This is a region of high current density. As shown in the turbulent photograph, the discharge had become even more diffused. The bright region at the tips of each pin was wider and visibly more dispersed. The localized current density in this region has become more diffused due to turbulent mixing. Similar observations are reported in Reference 3. The outer or periphery pins of the anode were the first pins to develop the intense bright region described above. The center pins did not "light up" as brightly as the outer pins.

VI. CONCLUSIONS AND RECOMMENDATIONS

Even though maximum operating conditions were not reached due to power supply current limitations, sub-ambient, controlled turbulent flow had a significant effect on discharge stability in the working range of this experiment. Turbulence generating plates must be kept in the immediate vicinity of the discharge (location C, Fig. 3) to avoid spectral decay in a wind-tunnel contraction. Power input is scalable with mass flow rate. The combined effect of reduced pressure and turbulent flow at maximum performance obtained in this experiment was to increase discharge power by 750% over ambient laminar flow at the same mass flow rate.

The upper limit of power input for this apparatus would occur under choke conditions with Plate III installed at location C, but a power supply with sufficient output would be needed to reach that level. The slope of the turbulent flow curves may or may not eventually decrease in the same manner as the "laminar" curves, and this needs to be further investigated. Turbulence spectrum data could be enhanced by laser velocimeter measurements of the turbulent flow.

At a given average discharge velocity the total discharge power can be obtained from Figure 16 for either the turbulent or "laminar" case. This power is represented by a line of constant power in Figure 15. The intercepts of this constant power line give mass flow rates corresponding to the diffuser on or off configuration. Since discharge area and velocities are equal, only density accounts for the difference in mass flow rates. This conclusion is supported by the data.

By extrapolating the probable path of the "laminar" curves in Figure 14 (see Fig. 20), decreasing density ratio versus total discharge power can be projected. The ratio of mass flow rates corresponding to the intercepts of constant power lines gives ρ / ρ_o. The resulting curve is shown in Figure 21.

There are a number of improvements that can be incorporated into this apparatus. As mentioned earlier, a larger power supply would vastly improve the capability of the system. This would also require additional electric shielding of the high voltage circuit to protect the operators. The center row of anode pins had a glow intensity less than the periphery pins for all flow and no-flow tests. This may have been influenced by the cathode wire

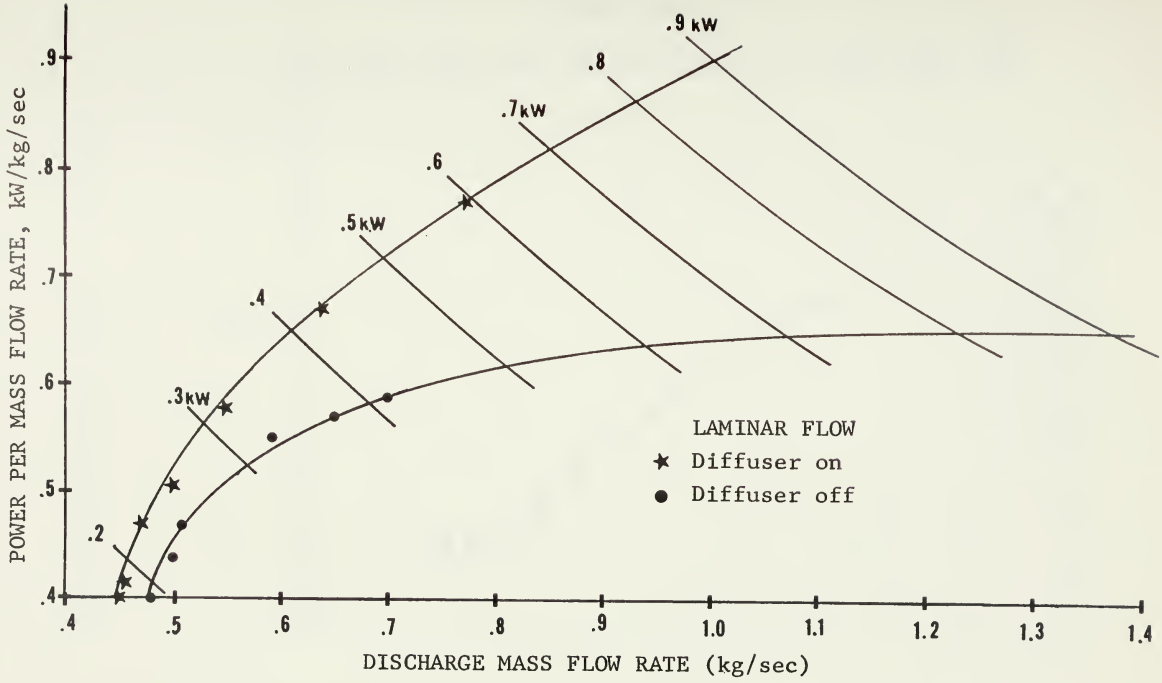

Figure 20. Extrapolated Laminar Curves

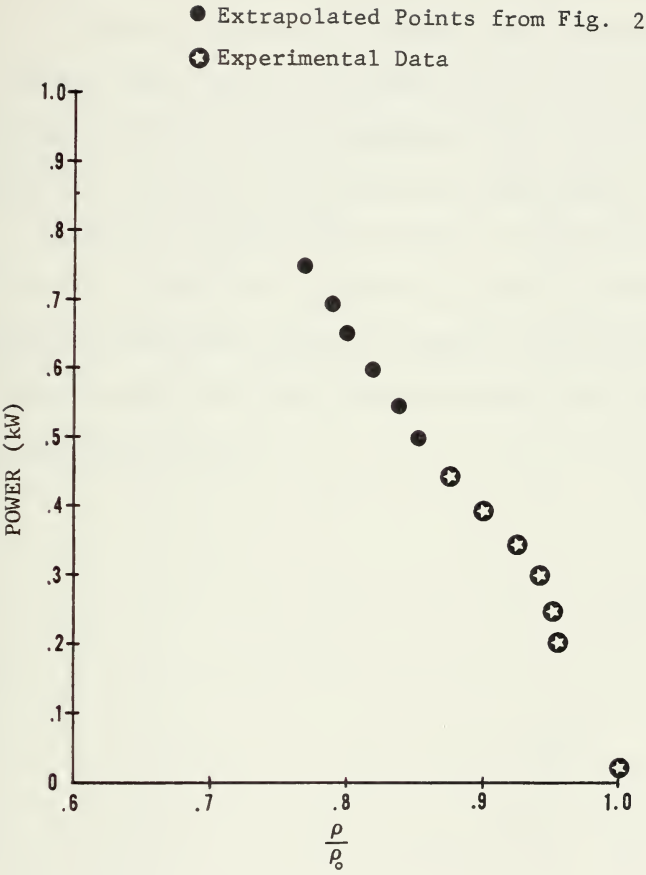

Figure 21. Power Versus Density Ratio

grid frame. Optimizing pin density for turbulent flow may also produce interesting results. An electrode gap length of 2.9 cm was used for all discharge data presented. With a larger power supply the optimum gap for the corresponding operating density of the discharge region could be experimentally determined and improve the performance.

A closed, pressure tight system as suggested by Reference 11 would alleviate the problem of relative humidity and would provide independent control of density and velocity. A closed system would also enable economic use of valuable lasing gas mixtures.

APPENDIX A

PARTIAL PRESSURE OF WATER VAPOR IN DISCHARGE

The relative humidity and temperature of ambient air determines the partial pressure of water vapor at the compressor inlet by using

$$(1) \qquad P_w = \Phi P_g$$

where P_w is the partial pressure of water vapor, Φ is the relative humidity and P_g is the saturation pressure determined from steam tables. A detailed steam table can be found in Reference 14. From Dalton's Law,

$$(2) \qquad P = P_w + P_a$$

where the subscript a refers to the partial pressure of dry air. The specific humidity is given by

$$(3) \qquad \Gamma = \frac{P_w}{P_a}\frac{M_w}{M_a} = 0.621\,\frac{P_w}{P_a} \qquad \frac{\text{LB OF WATER}}{\text{LB OF AIR}}$$

M_w and M_a are the molecular weights of water and air respectively.

From Eqs. (1) and (2), and measured ambient pressure, P_a can be determined, which in turn, when substituted into Eq. (3) will give the specific humidity of the flow. The specific humidity will remain unchanged provided condensation

does not occur. If the flow temperature drops below the local dew point, condensation will take place and, therefore, reduce Γ.

To determine the partial pressure of water vapor in the discharge region, the static pressure and temperature of the test section were measured. Assuming for the present Γ remained constant, Eqs. (2) and (3) are used to determine P_w in the test section.

$$(4) \qquad P_a = \frac{P}{(1 + \Gamma/0.621)}$$

$$(5) \qquad P_w = \frac{P_a}{0.621}$$

The steam tables were used to determine P_g in the test section and substituted into Eq. (1) to determine the relative humidity. If the calculated Φ was greater than or equal to one, Γ had decreased or was about to and the partial pressure of water vapor in the discharge region, P_w, was equal to P_g. If Φ was less than 1, the partial pressure of water vapor as calculated in Eq. (5) was correct.

A corresponding breakdown correction factor was then determined from Figure 22. All data was corrected to standard humidity conditions.

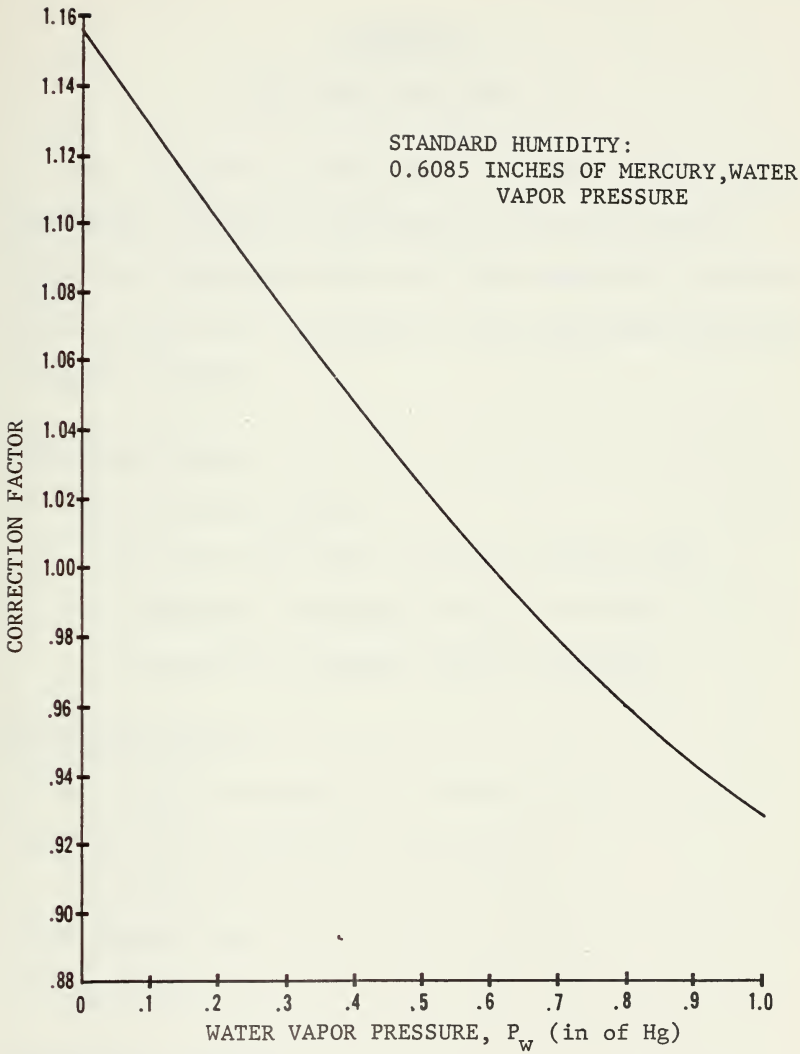

Figure 22. Relative Humidity Correction Curve (Ref. 9)

APPENDIX B

ERROR ANALYSIS (REF. 15)

The uncertainty of the results depended on accurate measurement readings of breakdown voltage and current, total flow temperature and static and stagnation pressures. The following is an estimation of the uncertainty interval of these variables.

Breakdown voltage:

$V_b = (V \pm 0.2)\ 0.99$ kV

The 0.99 comes from using the control panel voltmeter. Breakdown voltage was first corrected to standard relative humidity.

Breakdown current:

$I_b = I \pm 0.2$ mA for $0 < I < 10$ mA

$I_b = I \pm 1.0$ mA for $10 < I < 24$ mA

Total Temperature:

$T_o = T \pm 2\ ^{o}R$

Stagnation Pressure:

$P_o = p \pm 0.005$ PSIA for H_2O manometers

$P_o = p \pm 0.02$ PSIA for Hg manometers

Static Pressure:

$p_s = p \pm 0.005$ PSIA for H_2O manometers

$p_s = p \pm 0.02$ PSIA for Hg manometers

The intermediate results are functions of the test variables as stated below.

Power:

$P = VI$ watts

Flow Temperature:

$T = T(T_o, p_o, p_s)$ isentropic

Velocity:

$v = v(T_o, p_o, p_s)$ isentropic

Density:

$\rho = \rho(T_o, p_o, p_s)$ isentropic

First, consider the uncertainty in experimental values of power.

1) $P = VI$ watts

2) $P + \Delta P = 0.99 (V + \Delta V) (I + \Delta I)$

Subtracting eq. 1) from 2) gives

$\Delta P = 0.99 (VI + V \Delta I + I \Delta V + \Delta V \Delta I) - 1$

$\Delta P = -0.01 VI + 0.99 (V \Delta I + I \Delta V)$

$\frac{\Delta P}{P} = 0.99 (\frac{\Delta I}{I} + \frac{\Delta V}{V}) -0.01$

In a similar manner the uncertainty interval was determined for the remaining test quantities and are summarized below.

Flow Temperature:

$$\frac{\Delta T}{T} = \frac{T_o + \Delta T_o}{\left(\frac{P_o \mp | \Delta P_o |}{P_s \pm | \Delta P_s |} \right)^{0.29}} - 1 \quad , \qquad T \left[{}^{o}R \right]$$

Velocity:

$$\frac{\Delta v}{v} = \frac{1}{v} \left\{ 12015.08 \, (T_o + \Delta T_o) \left[1 - \left(\frac{P_s \mp | \Delta P_s |}{P_o \pm | \Delta P_o |} \right)^{0.29} \right] \right\}^{0.5} - 1$$

$$v \left[\text{ft/sec} \right]$$

Density:

$$\frac{\Delta \rho}{\rho} = \frac{2.70}{\rho} \left[\frac{P_s \pm | \Delta P_s |}{T \mp | \Delta T |} \right] - 1, \qquad \rho \left[\frac{\text{lbm}}{\text{ft}^3} \right]$$

Mass Flow Rate:

$$\frac{\Delta \dot{M}}{\dot{M}} = \frac{\Delta \rho}{\rho} + \frac{\Delta v}{v}, \qquad \dot{M} \left[\frac{\text{lbm}}{\text{sec}} \right]$$

LIST OF REFERENCES

1. Fuhs, A. E., unpublished lecture notes from course AE 4505, Laser Technology, given at the Naval Postgraduate School, 1975.

2. Biblarz, O. and Nelson, R. E., "Turbulence Effects of an Ambient Pressure Discharge," Journal of Applied Physics, v. 45, p. 633, Feburary 1974.

3. Wiegand, W. J. and Nighan, W. L., "Influence of Fluid Dynamic Phenomena on the Occurrence of Constriction in cw Convection Laser Discharges," Applied Physics Letter, v. 26, p. 554, 1975.

4. Wasserstron, E., Crispin, Y., Rom, J. and Shwartz, J., The Interaction Between Electrical Discharges and Gas Flow, AIAA Paper 76-315, American Institute of Aeronautics and Astronautics, New York, 1976.

5. Shwartz, J. and Wassertrom, E.,"The Role of Gas Flow and Turbulence in Electric Discharge Lasers," Israel Journal of Technology, v. 13, p. 122-133, May 1975.

6. Loeb, L. B., Electrical Coronas, p. 110, University of California Press, 1965.

7. Barto, J. L., Gasdynamic Effects on an Electric Discharge in Air, MS Thesis, Naval Postgraduate School, Monterey, California, 1976.

8. Tennekes, H. and Lumley, J. L., A First Course in Turbulence, p. 81-84, MIT Press, 1972.

9. Cobine, J. D., Gaseous Conductors, Theory and Engineering Applications, p. 181-183, McGraw-Hill, 1941.

10. Phelps, C. T. and Griffiths, R. J., "Dependence of Positive Corona Streamer Propagation on Air Pressure and Water Vapor Content," Journal of Applied Physics, v. 47, p. 2929, July 1976.

11. Aunchman, L. J. Jr., Controlled Turbulence as a Design Criterion for Electric Discharge Convection Lasers, MS Thesis, Naval Postgraduate School, Monterey, California, March 1974.

12. Shapiro, A. H., The Dynamics and Thermodynamics of Compressible Fluid Flow, v. 1, p. 83-87, Ronald Press, 1953.

13. Shih, C. C., (private communication).

14. Smithsonian Meteorological Tables, 6th ed., p. 351-359, Smithsonian Institution, 1951.

15. Miller, J. A., unpublished lecture notes from course AE 2806, Aeronautical Labs II, given at the Naval Postgraduate School, 1975.

INITIAL DISTRIBUTION LIST

		No. Copies
1.	Defense Documentation Center Cameron Station Alexandria, Virginia 22314	2
2.	Library, Code 0212 Naval Postgraduate School Monterey, California 93940	2
3.	Department Chairman, Code 67 Department of Aeronautics Naval Postgraduate School Monterey, California 93940	1
4.	Professor O. Biblarz Department of Aeronautics Naval Postgraduate School Monterey, California 93940	2
5.	LT Howard A. Post, USN Navy Space System Activity Air Force Unit Post Office Los Angeles, California 90045	1
6.	LCDR J. L. Barto, USN 960 C Avenue Coronado, California 92118	1
7.	Dr. D. G. Samaras Air Force Office of Scientific Research (AFSC) Bolling AFB Washington, D. C. 20332	1
8.	Dr. J. Shwartz, R1-1016 TRW One Space Park Redondo Beach, California 90278	1
9.	Professor C. C. Shih Department of Mechanical Engineering The University of Alabama at Huntsville P. O. Box 1247 Huntsville, Alabama 35807	1

10. Dr. H. H. Legner 1
AVCO-Everett Research Laboratory
2385 Revere Beach Pkwy.
Everett, Massachusetts 02149

11. Dr. Allan Garscadden 1
Plasma Physics Research Laboratory
ARL (LU), Bldg. 450
Wright-Patterson AFB, Ohio 45433

Thesis
P74825 Post
c.1

166762

Sub-ambient controlled turbulence effects on discharge stabilization for laser applications.